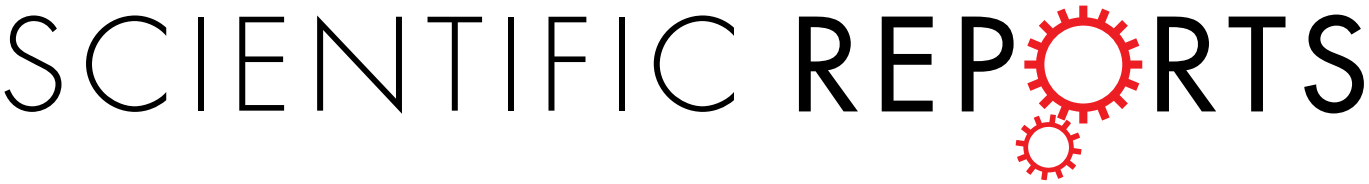

OPEN

Switching Behaviors of Graphene-Boron Nitride Nanotube Heterojunctions

Received: 11 January 2015
Accepted: 23 June 2015
Published: 20 July 2015

Vyom Parashar[1], Corentin P. Durand[2], Boyi Hao[1], Rodrigo G. Amorim[1], Ravindra Pandey[1], Bishnu Tiwari[1], Dongyan Zhang[1], Yang Liu[3], An-Ping Li[2] & Yoke Khin Yap[1]

High electron mobility of graphene has enabled their application in high-frequency analogue devices but their gapless nature has hindered their use in digital switches. In contrast, the structural analogous, *h*-BN sheets and BN nanotubes (BNNTs) are wide band gap insulators. Here we show that the growth of electrically insulating BNNTs on graphene can enable the use of graphene as effective digital switches. These graphene-BNNT heterojunctions were characterized at room temperature by four-probe scanning tunneling microscopy (4-probe STM) under real-time monitoring of scanning electron microscopy (SEM). A switching ratio as high as 10^5 at a turn-on voltage as low as 0.5V were recorded. Simulation by density functional theory (DFT) suggests that mismatch of the density of states (DOS) is responsible for these novel switching behaviors.

Graphene is known for its high electron mobility and zero energy gap nature[1,2]. These have enabled their application in high-frequency analogue devices but hindering their use in digital switches[3]. Extensive efforts have been dedicated to generate band gap in graphene by using graphene nanoribbons[4,5], graphene bilayer[6,7], graphene on *hexagonal* phase boron nitride (graphene/*h*-BN)[8], and applying strain on graphene/*h*-BN structures[9]. In contrast, *h*-BN sheets and BN nanotubes (BNNTs) are insulators[10,11]. The *h*-BN substrates are known to enhance electron mobility of graphene devices[12,13]. More recently, in-plane graphene/*h*-BN heterojunctions were also reported[14–16]. However, graphene digital switches have not been demonstrated in any of these graphene/*h*-BN heterostructures. Here we show that zero dimensional (0D) heterojunctions between BNNTs and graphene could switch current flows.

The graphene-BNNT heterojunctions are prepared by chemical vapor deposition (CVD)[17,18], where BNNTs are grown on chemically exfoliated graphene without the use of catalysts (see Methods and Supplementary Fig. S1,S2). As shown in Fig. 1a,b, BNNTs were selectively grown on the graphene sheet and not on the surrounding oxidized Si substrates. The as-grown BNNTs point outward from the graphene surface at random angles. As shown in Fig. 1c,d, the self-assembled BNNTs are crystalline with tubular structure (Fig. S3), similar to those grown with the use of catalysts[11]. Raman spectroscopy (Fig. 1e, excitation laser wavelength = 325 nm), and electron energy loss spectroscopy (EELS, Supplementary Fig. S4) confirm the presence of BNNTs on graphene. The Raman spectra of the multilayered graphene before the BNNT growth are shown in the inset for comparison.

The as-grown graphene-BNNT heterojunctions were characterized for their electronic properties at room temperature by using a four-probe scanning tunneling microscopy (4-probe STM) system (see Methods)[19]. The 4-probe STM system allows us to observe the exact probing locations prior to current-voltage (*I-V*) measurements with the *in situ* SEM. Figure 2a shows an upright BNNT grown from the graphene surface. This BNNT was probed by a tungsten STM probe **1**, while another STM probe **2** was in contact with the graphene surface. The distance, *d*, between probe **1** and the vertical graphene-BNNT heterojunction, was controlled by changing the contact point on the BNNT.

[1]Department of Physics, Michigan Technological University, 1400 Townsend Drive, Houghton, Michigan 49931, USA. [2]Center for Nanophase Materials Sciences, Oak Ridge National Laboratory, Oak Ridge, TN 37831-6487, USA. [3]Center for Integrated Nanotechnologies, Sandia National Laboratories, Albuquerque, NM 87185. Correspondence and requests for materials should be addressed to Y.K.Y. (email: ykyap@mtu.edu)

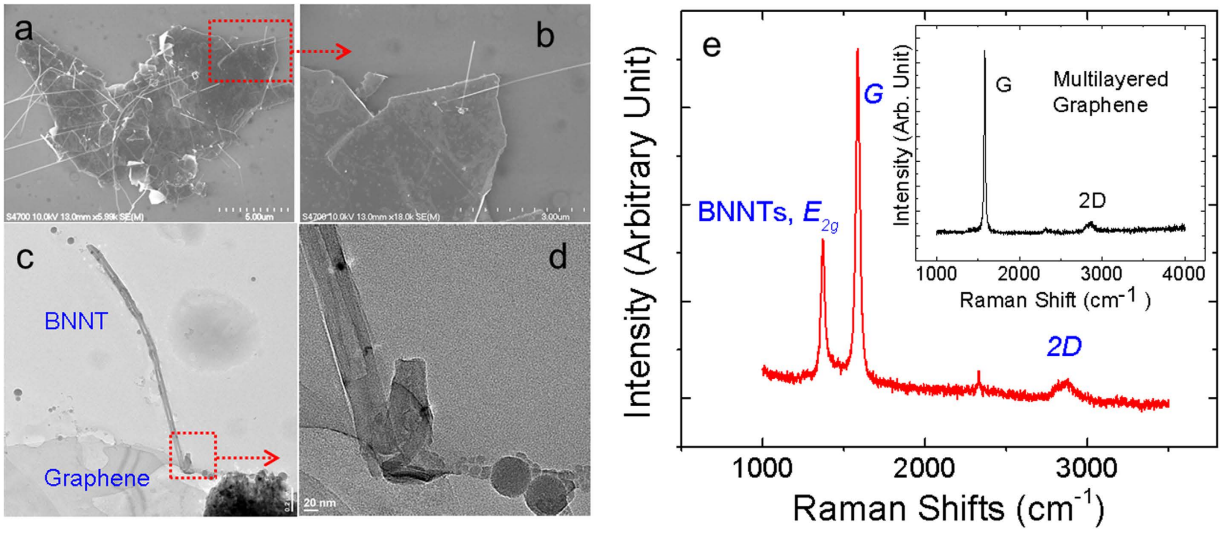

Figure 1. Structural Properties of graphene-BNNT heterojunctions. Microscopic images of graphene-BNNT heterojunctions obtained by (**a,b**) scanning electron microscopy (SEM) and (**c,d**) transmission electron microscopy (TEM). (**e**) Raman spectra obtained from as-grown graphene-BNNTs in comparison with the spectra from the multilayered graphene (inset). The diameters of these BNNTs are typically 20–80 nm.

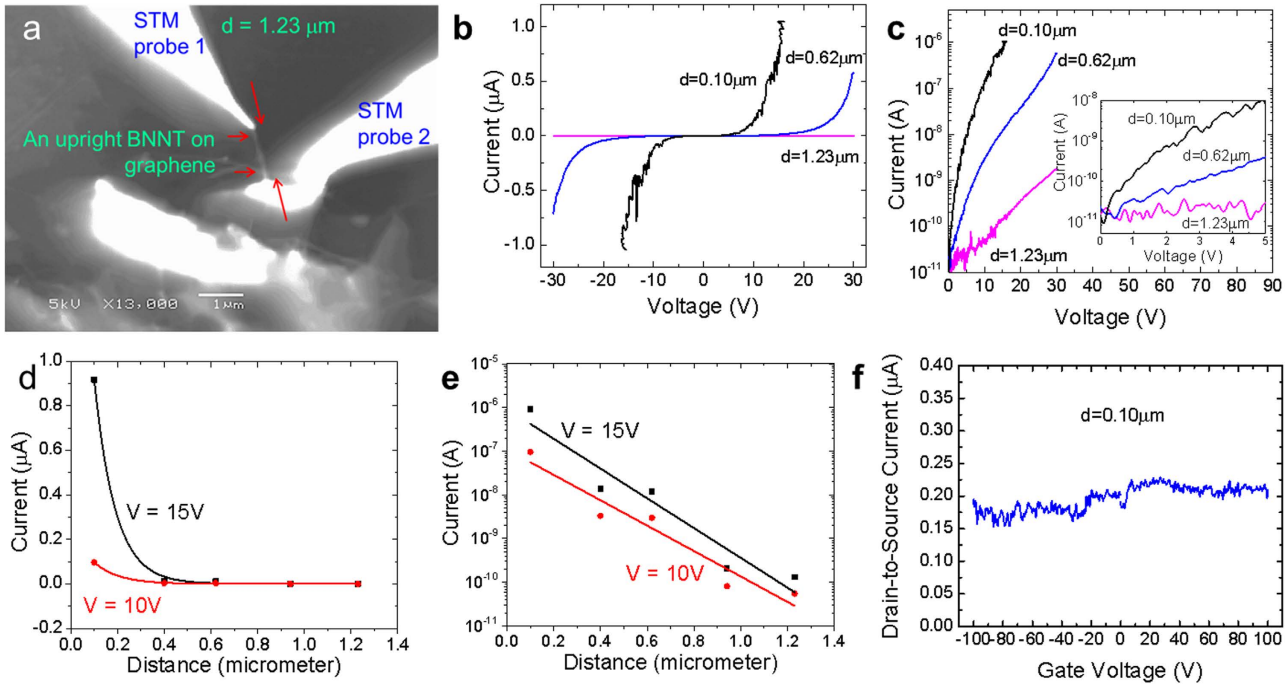

Figure 2. Distance dependent transport properties on a vertical heterojunction. (**a**) SEM image of a graphene-BNNT heterojunction as contacted across by two STM probes at conduction distance, $d = 1.23\,\mu m$. (**b,c**) The corresponding current-voltage (I-V) characteristics at a series of d. (**d,e**) Linear and log scale of current flow across the heterojunction as a function of distance, d as extracted from Fig. S8. (**f**) The source-drain currents across the heterojunction as a function of back gate voltages.

For the case of $d = 1.23\,\mu m$, we hardly detected any current flow across the graphene-BNNT heterojunction for a range of bias voltages, V_b (Fig. 2b,c) between -30 V and $+30$ V. The current noise level (i.e. "off" state) is about ~10^{-11}A. As we changed d to $0.62\,\mu m$, we detected a significant higher level of current across the heterojunction (i.e. "on" state) with a threshold turn–on voltage, V_{on} ~0.5 V (inset). The current level detected at $d = 0.10\,\mu m$ is even higher, up to μA level (as limited by the preset 1 μA current

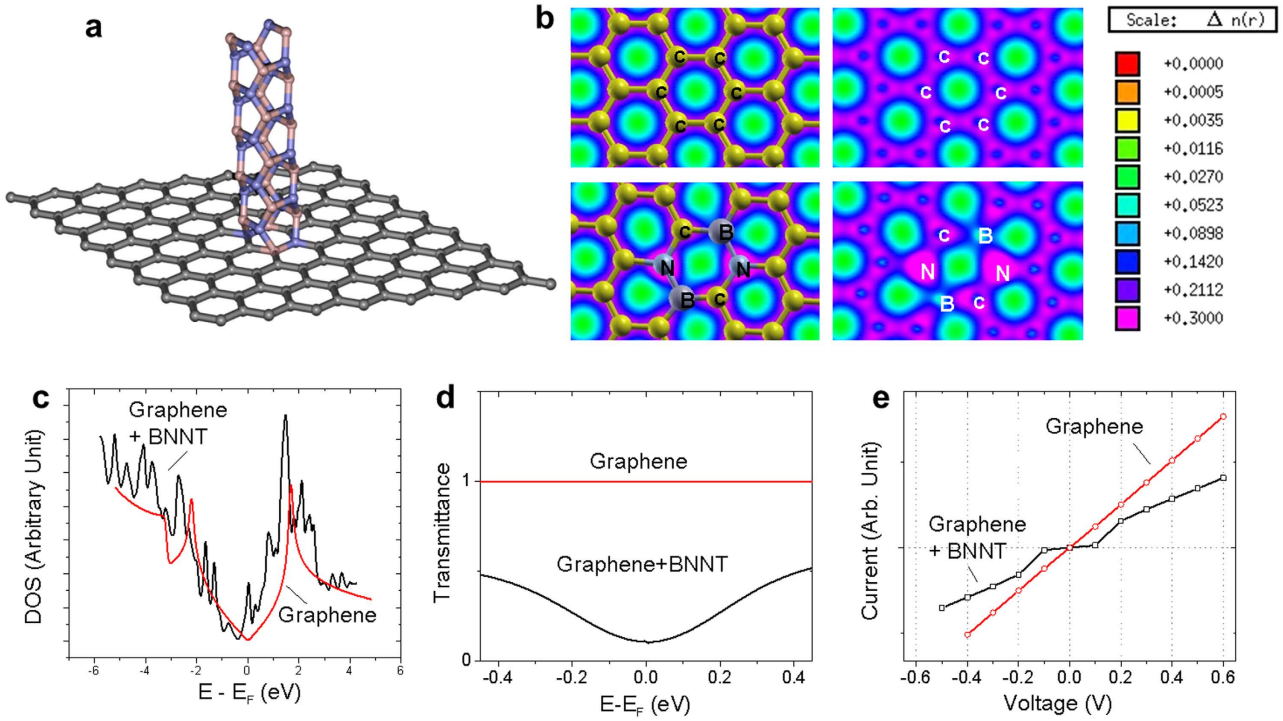

Figure 3. Theory. (a) Model of a vertical graphene-BNNT heterojunction. **(b)** Electron charge density of the pristine graphene (upper row) and the graphene-BNNT heterojunction (lower row). (**c**) Density of states (DOS), (**d**) the transmittance at zero bias, and (**e**) the current-voltage characteristics of the pristine graphene (upper row) and the graphene-BNNT heterojunction.

limit), with V_{on} ~0.15 V (inset). These conducting behaviors with obvious "on" and "off" states are different from the reported insulating nature of BNNTs[18,20]. Such a switching behavior is also different from the metallic nature detected when both STM probes are in contact with the graphene surface (Fig. S7). These results suggest that graphene-BNNT heterojunctions could be used as electronic switches with an estimated switching ratio of 10^5.

A full series of *I-V* curves were measured (supplementary Fig. S8). The detected current as a function of *d* at bias voltage V = 10 V and 15 V are extracted and plotted on two different scales in Fig. 2d,e, respectively. As shown, current across the graphene-BNNT heterojunctions decreased nonlinearly with the increase in the probe-heterojunction tunneling distance, *d*. Next, we investigated the gating effect on this vertical graphene-BNNT heterojunction. By keeping V_b ~10 V at $d = 0.10\,\mu$m, the current flow across the heterojunction was monitored while applying a varying back gate voltage on the highly doped *p*-type Si ⟨100⟩ substrate (0.001–0.005 Ωcm, with a 500 nm thick Si oxide layer on top). As shown in Fig. 2f, a nearly constant current of 10^{-7}A is detected. We believe that the absence of the gating effect is due to the shielding of the metallic graphene located between the gate oxide surface and the heterojunction. As the junction is small in diameter (~60 nm) and is potentially surrounded by additional graphene layers underneath, an electrostatic screening effect will be able to effectively shield the gating effect. Therefore, gating the junction should still be possible if a top gate is applied.

To understand these experimental observations, calculations were performed by employing Density Functional Theory (DFT)[21,22] as implemented in the SIESTA code (see supplementary)[23]. The graphene-BNNT heterojunction was modeled in a supercell consisting of a graphene sheet and a BNNT placed perpendicular to the graphene sheet as shown in Fig. 3a. The calculated electron charge density for pristine graphene (upper row) and the graphene-BNNT heterojunction (lower row) is displayed in Fig. 3b. Here, a higher charge density is seen around the N atoms relative to that around the B atoms as expected. The calculated density of states (DOS) of the heterojunction together with the pristine graphene is shown in Fig. 3c. The shape of Dirac cones is well reproduced for the pristine graphene. On the other hand, DOS for the graphene-BNNT heterojunction is slightly shifted relative to that of the pristine graphene due to hybridization of C states with B/N states. Additional localized states are also predicted. There is an obvious mismatch of DOS at the nanoscale heterojunction between the graphene and the BNNT.

Next we calculated the electron transport properties of the heterojunctions using density functional theory together with the non-equilibrium Greens Function method (see supplementary). Fig. 3d shows the electronic transmittance at zero bias for both pristine graphene and graphene-BNNT heterojunction.

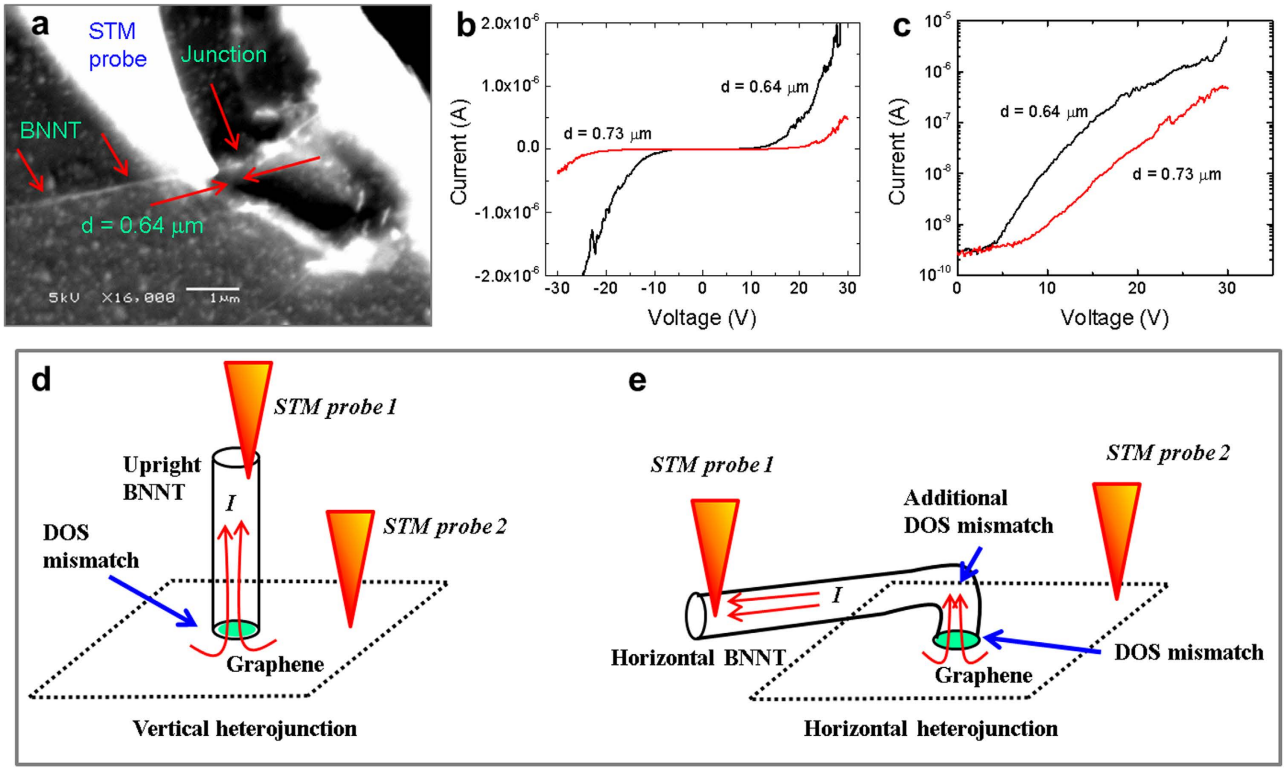

Figure 4. Distance dependent transport properties on a horizontal heterojunction and the schematic of DOS mismatch. SEM images of a horizontal graphene-BNNT heterojunction as contacted across by two STM probes (**a**) and the current-voltage (*I-V*) characteristics (**b,c**) at $d = 0.73\,\mu m$, and $d = 0.64\,\mu m$. Schematic drawing of a vertical heterojunction (**d**) and horizontal heterojunction (**e**) indicate the locations of DOS mismatch.

The ballistic nature in pristine graphene is clearly predicted with a flat transmittance at the conducting range. For the heterojunction, the transmittance is suppressed, approaching zero at the Fermi level. The calculated *I-V* characteristics of pristine graphene and graphene-BNNT heterojunction are shown in Fig. 3e. The Ohmic-like *I-V* behavior for the pristine graphene is predicted affirming its metallic nature. On the other hand, the calculations predict very little, if any, electron transport through the graphene-BNNT heterojunction within a range of low bias voltages (i.e. ± 0.1 V). At higher bias voltage, however, the linear *I-V* behavior is recovered with slightly higher resistance. The calculated switching properties of the heterojunction are in qualitative agreement with our experimental results.

We believe that the switching behaviors observed here is due to the DOS mismatch at the heterojunction[24], as shown in Fig. 3c,d. Such a mismatch creates a potential barrier and prevents current flows through the heterojunction at low bias. At higher bias voltages, an enhanced electric field is expected as the potential gradient is confined at the nanoscale heterojunction, much like in electron field emission[25]. This enables electrons to either overcome or tunnel through the mismatch barrier, leading to current flow across the heterojunction. The dimension of such a heterojunction is small, approaching zero dimensional (0D) structures. Considering the most effective switching case at $d = 0.10\,\mu m$, the effective dimension of the junctions is approximately ~120 nm in diameter.

We further examined the switching behavior of a horizontal graphene-BNNT heterojunction. Figure 4 shows the SEM image of a BNNT that is nearly horizontally extended from a graphene-BNNT heterojunction on to the surface of the oxidized Si substrate. As shown in Fig. 4a, an STM probe is in contact and pressing down the BNNT at a distance $d = 0.64\,\mu m$ away from the heterojunction. Another STM probe is in electrical contact with the graphene sheet (beyond the SEM imaging window). As shown in Fig. 4b,c, no significant current is detected at low V_b ("off" state) for both cases. At higher V_b, the heterojunction turned "on" with thresholds V_{on} ~7 V and V_{on} ~4 V for $d = 0.73\,\mu m$ and $0.64\,\mu m$, respectively. Obviously, V_{on} for this horizontal heterojunction is higher than those discussed for a vertical heterojunction shown in Fig. 2. As schematically shown in Fig. 4d,e, bending BNNT will locally distort the tubular structure. Theoretically, such a radially deformed BNNT segment is known to change the band structure and reduce the band gap of BNNTs[26]. This additional DOS mismatch can increase the potential barrier, leading to higher V_{on}. Such a DOS mismatch can only be artificially formed if local compression or severe bending occurs to the BNNT. It is unlikely to find such a deformation in as-grown BNNTs.

In conclusion, we have demonstrated the fabrication of the stable graphene-BNNT heterojunctions without the use of catalyst. A bias-dependent switching behavior has been observed at the heterojunctions. DOS mismatch between graphene and BNNT at the nanoscale heterojunction is suggested to prevent current flow at low bias voltages, and turn on the current flow at higher applied bias. The novel Graphene-BNNT heterojunctions would likely combine the advantage of the ballistic nature of electron mobility[27] of single layer graphene and the switchable transport properties, when CVD synthesis of single-wall BNNTs is established in the field.

Methods

Synthesis of graphene-BNNT heterojuctions. Expandable graphite powders (Grade 3772, >98% carbon, Anthracite Industries, Inc., a subsidiary of Asbury Carbons, expansion ratio ~1:300) were heat shocked into multi-layered graphene at 1000 °C in Argon ambient. These graphene sheets are then dispersed in tetrahydrofuran or isopropyl alcohol by sonication (10 minutes in a sonication bath). The suspended graphene was then coated on cleaned oxidized Si substrates and dried in hydrogen flow at 800 °C for 30 min. These graphene coated substrates are then used for the subsequence growth of BNNTs to form the heterojunctions. The growth of BNNT on graphene is based on our reported growth vapor trapping (GVT) chemical vapor deposition (CVD) method without the use of catalyst. These substrates were placed on the top of an alumina combustion boat in which B, MgO, and FeO precursors are loaded (total weight of 500 mg, with a mass ratio of 4:1:1). This setup was placed inside a closed-end quartz tube in the horizontal tube furnace with the graphene sheets facing upward. The precursors and substrates were then heated up to 1100–1200 °C with an ammonia flow of 200–350 sccm and kept for 30 min. Images of as-grown graphene-BNNTs heterojunctions are shown in Fig. S1 and Raman spectra of these heterojunctions are shown in Fig. S2. We believe that the growth of BNNTs is initiated by point defects, where dangling bonds serve as the nucleation sites. As some of the point defects are not round, the initially grown BNNTs became distorted (whitish dot in Fig. 1b, and Supplementary Fig. S3) but later converted into straight BNNTs as observed by transmission electron microscopy (TEM, Fig. 1c,d). These point defects are formed during the heat induced chemical expansion and exfoliation process. This interpretation is supported by the fact that BNNTs could not be grown on CVD graphene (Supplementary Fig. S5,S6). Apparently, the formation of graphene-BNNT junctions relies on the diameters of the point defects. We think that it is possible to form the graphene-BNNT heterojunction on mono- and multi-layered graphene (at a reasonable range of graphene thickness of ~0.4–30 nm to match the diameter of typical single- and multi- walled BNNTs) as long as the point defects are found.

References

1. Novoselov, K. S. *et al.* Electric field effect in atomically thin carbon films. *Science* **306,** 666–669 (2004).
2. Berger, C. *et al.* Ultrathin epitaxial graphite: 2D electron gas properties and a route toward graphene-based nanoelectronics. *J Phys Chem B* **108,** 19912–19916 (2004).
3. Schwierz, F. Graphene transistors. *Nat Nanotechnol* **5,** 487–496 (2010).
4. Han, M. Y., Ozyilmaz, B., Zhang, Y. B. & Kim, P. Energy band-gap engineering of graphene nanoribbons. *Phys Rev Lett* **98,** 206805 (2007).
5. Li, X. L., Wang, X. R., Zhang, L., Lee, S. W. & Dai, H. J. Chemically derived, ultrasmooth graphene nanoribbon semiconductors. *Science* **319,** 1229–1232 (2008).
6. Ohta, T., Bostwick, A., Seyller, T., Horn, K. & Rotenberg, E. Controlling the electronic structure of bilayer graphene. *Science* **313,** 951–954 (2006).
7. Zhang, Y. B. *et al.* Direct observation of a widely tunable bandgap in bilayer graphene. *Nature* **459,** 820–823 (2009).
8. Giovannetti, G., Khomyakov, P. A., Brocks, G., Kelly, P. J. & van den Brink, J. Substrate-induced band gap in graphene on hexagonal boron nitride: Ab initio density functional calculations. *Phys Rev B* **76,** 073103 (2007).
9. Zhong, X. L., Yap, Y. K., Pandey, R. & Karna, S. P. First-principles study of strain-induced modulation of energy gaps of graphene/BN and BN bilayers. *Phys Rev B* **83,** 193403 (2011).
10. Yap, Y. K. *B.-C.-N nanotubes and related nanostructures.* (Springer, 2009).
11. Wang, J. S., Lee, C. H. & Yap, Y. K. Recent advancements in boron nitride nanotubes. *Nanoscale* **2,** 2028–2034 (2010).
12. Dean, C. R. *et al.* Boron nitride substrates for high-quality graphene electronics. *Nat Nanotechnol* **5,** 722–726 (2010).
13. Mayorov, A. S. *et al.* Micrometer-Scale Ballistic Transport in Encapsulated Graphene at Room Temperature. *Nano Letters* **11,** 2396–2399 (2011).
14. Levendorf, M. P. *et al.* Graphene and boron nitride lateral heterostructures for atomically thin circuitry. *Nature* **488,** 627–632 (2012).
15. Liu, Z. *et al.* In-plane heterostructures of graphene and hexagonal boron nitride with controlled domain sizes. *Nat Nano* **8,** 119–124 (2013).
16. Liu, L. *et al.* Heteroepitaxial Growth of Two-Dimensional Hexagonal Boron Nitride Templated by Graphene Edges. *Science* **343,** 163–167 (2014).
17. Lee, C. H., Wang, J. S., Kayatsha, V. K., Huang, J. Y. & Yap, Y. K. Effective growth of boron nitride nanotubes by thermal chemical vapor deposition. *Nanotechnology* **19,** 455605 (2008).
18. Lee, C. H., Xie, M., Kayastha, V., Wang, J. S. & Yap, Y. K. Patterned Growth of Boron Nitride Nanotubes by Catalytic Chemical Vapor Deposition. *Chem Mater* **22,** 1782–1787 (2010).
19. Lee, C. H. *et al.* Room-Temperature Tunneling Behavior of Boron Nitride Nanotubes Functionalized with Gold Quantum Dots. *Adv Mater* **25,** 4544–4548 (2013).
20. Ghassemi, H. M., Lee, C. H., Yap, Y. K. & Yassar, R. S. Field emission and strain engineering of electronic properties in boron nitride nanotubes. *Nanotechnology* **23,** 105702 (2012).
21. Hohenberg, P. & Kohn, W. Inhomogeneous Electron Gas. *Physical Review* **136,** B864–B871 (1964).
22. Kohn, W. & Sham, L. J. Self-Consistent Equations Including Exchange and Correlation Effects. *Physical Review* **140,** A1133–A1138 (1965).
23. Soler, J. M. *et al.* The SIESTA method for ab initio order-N materials simulation. *J Phys-Condens Mat* **14,** 2745–2779 (2002).

24. Clark, K. W. *et al.* Energy Gap Induced by Friedel Oscillations Manifested as Transport Asymmetry at Monolayer-Bilayer Graphene Boundaries. *Physical Review X* **4,** 011021 (2014).
25. Pandey, A. *et al.* Very Stable Electron Field Emission from Strontium Titanate Coated Carbon Nanotube Matrices with Low Emission Thresholds. *ACS Nano* **7,** 117–125 (2012).
26. Kim, Y.-H., Chang, K. J. & Louie, S. G. Electronic structure of radially deformed BN and BC_3 nanotubes. *Phys Rev B* **63,** 205408 (2001).
27. Baringhaus, J. *et al.* Exceptional ballistic transport in epitaxial graphene nanoribbons. *Nature* **506,** 349–354 (2014).

Acknowledgments

This work is supported by the U.S. Department of Energy, Office of Basic Energy Sciences, Materials Sciences and Engineering Division (Grant DE-SC0012762). The theoretical effort is supported by the US Army Research Laboratory, Weapons and Materials Directorate "Hybrid Nano and Nano-Bio Materials" Program. Part of the experimental work was conducted at the Center for Nanophase Materials Sciences (Project CNMS2012-083), which is sponsored at Oak Ridge National Laboratory by the Scientific User Facilities Division, Office of Basic Energy Sciences, the U.S. Department of Energy. Part of this work was performed at the Center for Integrated Nanotechnologies (Project U2011A1074), an Office of Science User Facility operated for the U.S. Department of Energy, Office of Science by Los Alamos National Laboratory (Contract DE-AC52-06NA25396) and Sandia National Laboratories (Contract DE-AC04-94AL85000).

Author Contributions

V.P., B.H. and B.T. fabricated the materials; C.D., B.H., B.T., D.Y., Y.L. and Y.K.Y. performed the experimental measurements; R.A. and R.P. designed and performed the theoretical simulation. V.P., A-P.L. and Y.K.Y. designed the experiments. V.P., C.D., R.P., A-P. Li. and Y.K.Y. wrote the manuscript with input from all co-authors.

Additional Information

Supplementary information accompanies this paper at http://www.nature.com/srep

Competing financial interests: The authors declare no competing financial interests.

How to cite this article: Parashar, V. *et al.* Switching Behaviors of Graphene-Boron Nitride Nanotube Heterojunctions. *Sci. Rep.* **5**, 12238; doi: 10.1038/srep12238 (2015).

Supplementary Information

Switching Behaviors of Graphene-Boron Nitride Nanotube Heterojunctions

Vyom Parashar[1], *Corentin P. Durand*[2,], *Boyi Hao*[1], *Rodrigo G. Amorim*[1], *Ravindra Pandey*[1], *Bishnu Tiwari*[1], *Dongyan Zhang*[1], *Yang Liu*[3], *An-Ping Li*[2], *and Yoke Khin Yap*[1,*]

[1]Department of Physics, Michigan Technological University, 1400 Townsend Drive, Houghton, Michigan 49931, USA. [2]Center for Nanophase Materials Sciences, Oak Ridge National Laboratory, Oak Ridge, TN 37831-6487, USA. [3]Center for Integrated Nanotechnologies, Sandia National Laboratories, Albuquerque, NM 87185. [*]e-mail: ykyap@mtu.edu

1. Synthesis of graphene-BNNT heterojunctions

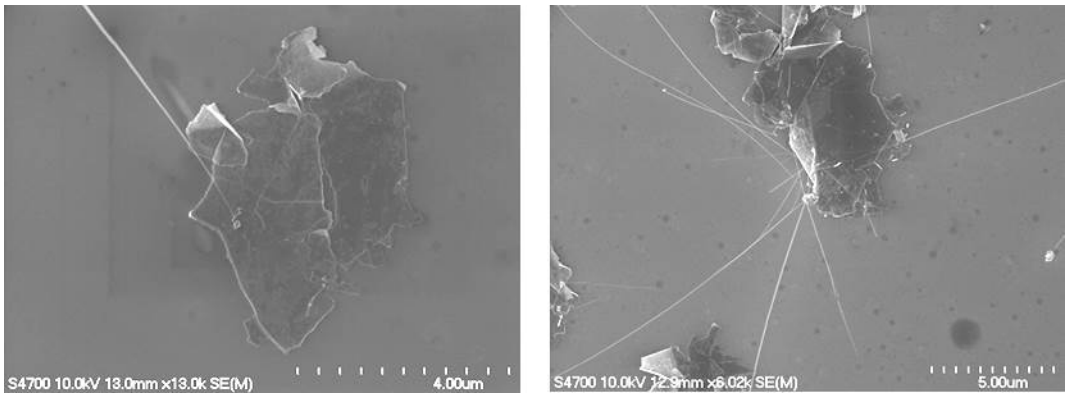

Figure S1: Additional SEM images of selectively grown graphene-BNNT heterojunctions.

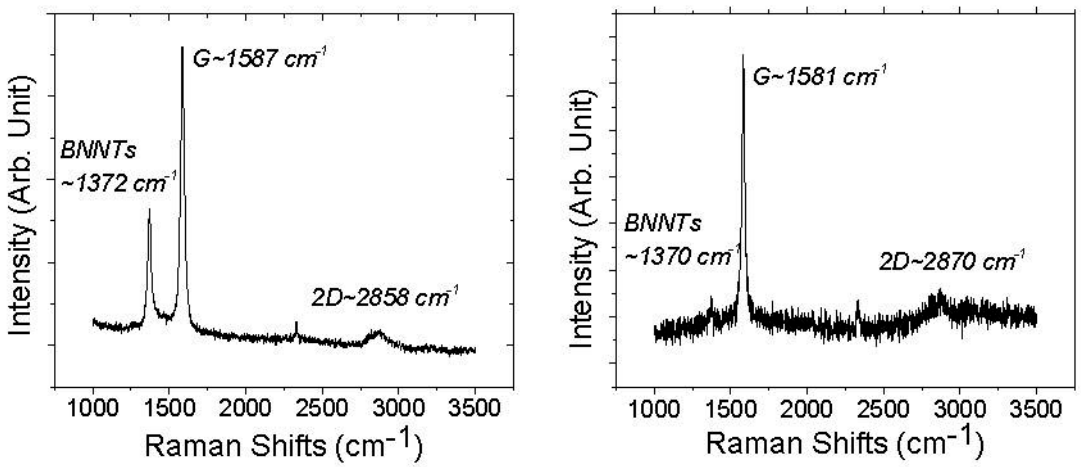

Figure S2: Raman spectra of graphene-BNNT heterojunctions with dense BNNTs (left) and sparse BNNTs (right). As shown the *G* and *2D* peak positions are varying with location while the BNNT peaks are about ~1370-1372 cm^{-1}.

The Raman G peak position for graphene is ~1580 cm^{-1} but can be varied by strains. [1] As shown in Figure S2, the G peak has significantly shifted when denser BNNTs are grown, potentially due to the strain induced by the formation of the heterojunctions. On the other hand, the Raman 2D peak position is very sensitive to the number of graphene layer as well as the wavelength of the excitation laser.[2] For example, 2D peak as excited by HeNe (633nm) laser is ~2640 cm^{-1} and will shift to ~2825 cm^{-1} when excited by HeCd (325nm) laser.[3] The 2D peak position can also be further shifted by strain.[1]

2. Transmission electron microscopy (TEM) and electron energy loss spectroscopy (EELS)

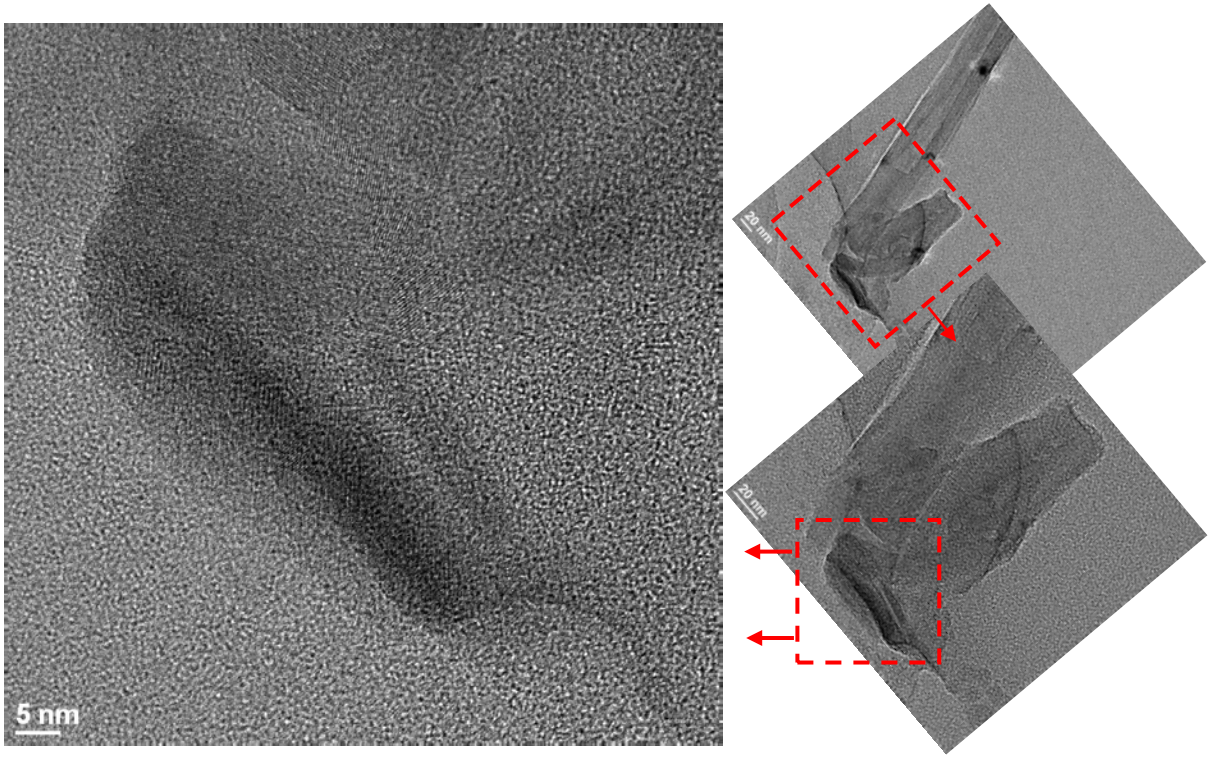

Figure S3: Lattice of randomly stacked hexagonal BN phase is detected at the graphene-BNNT junction.

TEM was employed to examine the structural properties at the graphene-BNNT heterojunction. A long BNNT and another broken BNNT are shown in Figure S3 (upper right). At the heterojunctions of graphene and these BNNTs, (lower right and left), highly crystalline hexagonal BN shells are detected in a randomly stacked manner. We interpret this as twisted / distorted tubular BN structure. Electron energy loss spectroscopy (EELS) was also employed to analyze the composites on the BNNTs and the graphene-BNNT heterojuction. As shown in Figure S4, the spectra for B, C, and N atoms are detected on the graphene-BNNT junction.

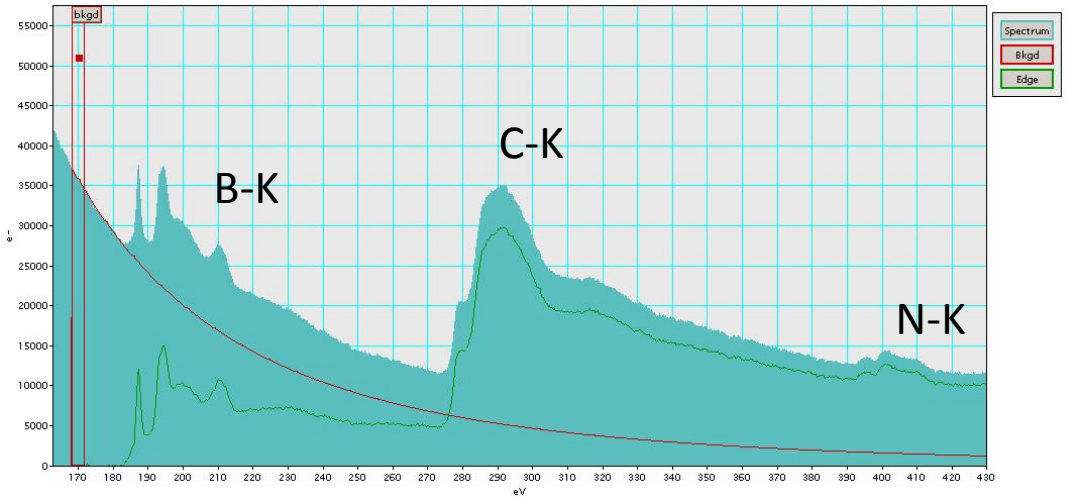

Figure S4: EELS spectra for B, C, N elements detected on the BNNT through the graphene layer.

3. Attempts to grow BNNTs on CVD graphene

We attempt to grow multiwalled graphene-BNNT heterojunctions using CVD graphene instead. These CVD graphene were grown on nickel (Ni) plates. These plates are cleaned by acetone, isopropyl alcohol, and then acetic acid, rinsed by DI water and blown dry with Ar before use. The Ni plates are heat treated in a CVD quartz chamber at 980°C for 10 mins under the flow of H_2 gas at a rate of 100 sccm. 20 sccm of CH_4 was then introduced for 25 mins. The growth was terminated by stopping the flows of H_2 and CH_4 gas. The furnace was then turned off and the

samples are cool down to room temperature in Ar ambient (300 sccm). These graphene samples were then examined by a confocal Raman spectroscopy system. Typical optical images of these graphene on Ni plates and the corresponding Raman spectra are shown in Figure S5. We then transfer the as-grown graphene from the Ni plate to oxidized Si substrates using thermal release tape (Semiconductor equipment Corp., #3195 MS). These graphene/Si samples are used for the subsequence growth of CVD BNNTs. As suggested by Raman spectroscopy and SEM imaging in Figure S6, we conclude that BNNTs could not be grown on these CVD graphene.

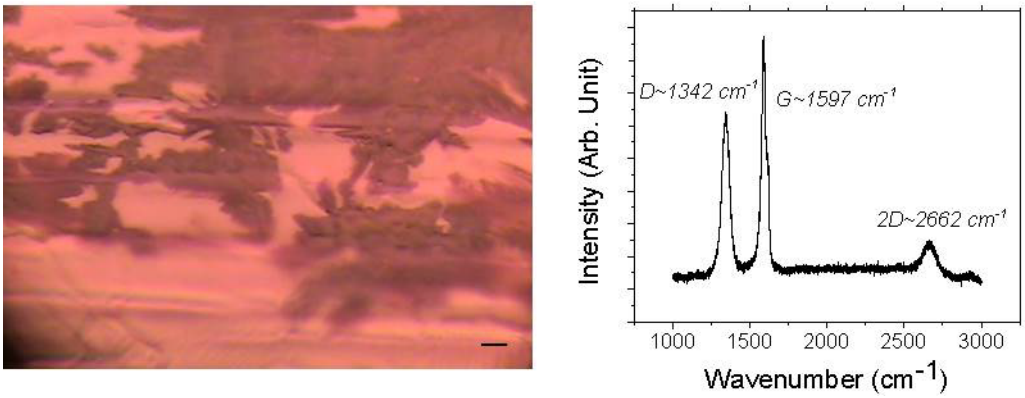

Figure S5: Optical Images of graphene grown on a Ni plate (left, scale bar = 2 μm) and the corresponding Raman spectra (right). As suggested by the Raman spectra, these are multilayered graphene.

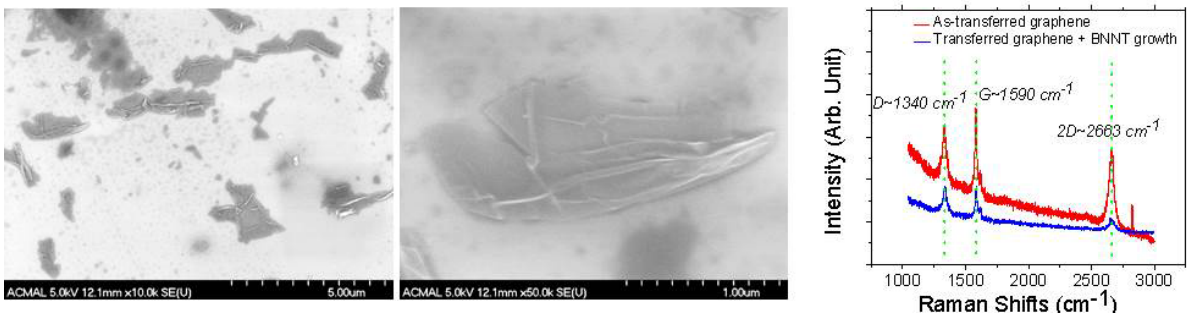

Figure S6: SEM images of the transferred graphene after BNNT growth. Raman spectra of the transferred graphene before and after the growth of BNNTs. No BNNTs are detected.

4. Characterization by four-probe scanning tunneling microscopy (4-probe STM)

All graphene-BNNT heterojunctions were characterized at room temperature using a 4-probe STM system under ultrahigh vacuum (base pressure $<2\times10^{10}$ Torr) at Oak Ridge National Laboratory's Center for Nanophase Materials Sciences. This system allows STM measurements and scanning electron microscopy (SEM) imaging. The as-grown graphene-BNNT heterojunctions on oxidized Si substrates (with 500 nm thermal oxide) were mounted on a sample stage, where gate potential can be applied in a back gate configuration. Electrochemically etched tungsten tips are used as the STM probes. After identifying an isolated heterojunction under SEM imaging, one tungsten probe was used to establish electrical contact on the graphene sheet with the guidance of the STM scanner. Another probe was directly contacted on the BNNT at a desired distance, *d* from the heterojunction. Potential differences were then applied across the two probes to characterize the room temperature transport properties across the graphene-BNNT heterojunctions. Figure S7 shows the linear current-voltage (*I*-*V*) characteristic of the graphene without contacting the BNNTs. This linear *I*-*V* behavior is very different from the switching characters across the graphene-BNNT junctions.

The STM system allows us to precisely control the Z position of the probes at an atomic resolution. This allows us to land our probes on graphene and BNNT surfaces in a controlled and reliable manner. For measurements on a heterojunction, we first make sure that Ohmic contacts can be obtained on the graphene as shown in Figure S7. Then, we keep one probe on a same spot of graphene, and use another probe to touch the BNNT at a minimum load. Pressing the BNNT harder can be easily observed under SEM as this will move the BNNT. Under excessive force, one can even see the bending of the BNNT and therefore can be easily avoided in our

experiments. In principle, our approach can eliminate the effect of contact resistance.

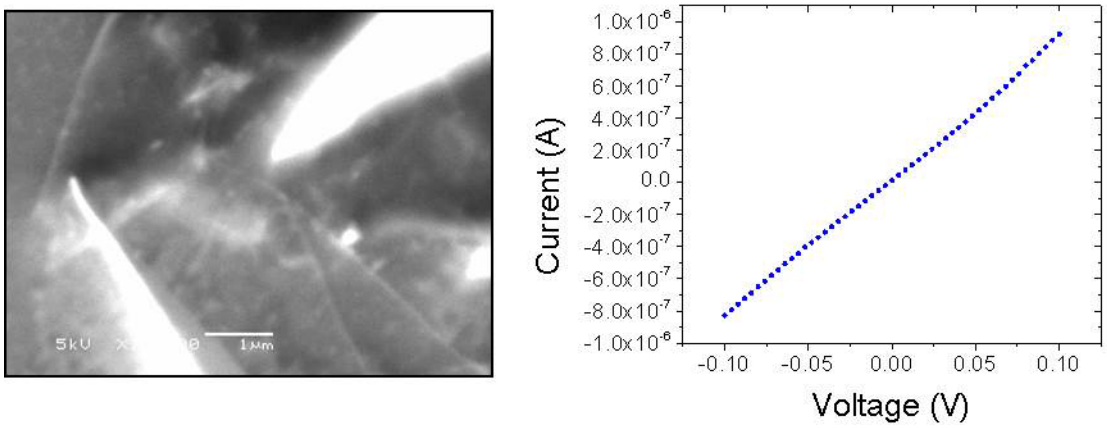

Figure S7. Two STM probes in contact with the graphene surface and the corresponding linear current-voltage (*I*-*V*) plot.

For the measurement on a vertical graphene-BNNT heterojunction, the STM probe was first approached near the surface of the sample and then lifted up until a contact with the freestanding BNNT was established. By monitoring the current noise level, we can tell when the STM probe is touching the vertically aligned BNNT as indicated by a sudden increase of the current noise level. By this way, we are sure that the STM probe is contact with the protruding BNNT and therefore confirm that it is a vertically aligned BNNT. The full data set of *I*-*V* characteristic across a vertical graphene-BNNT heterojunction at various distances *d* is shown in Figure S8a to S8e. As shown in Figure S8f and S8g, very low current are detected at d = 0.94 μm and 1.23 μm. *I*-*V* for d = 0.62 μm and 0.40 μm are quite identical. Much higher current are detected at d = 0.10 μm, and the *I*-*V* curve is very reproducible.

We further extracted data from Figure S8g, such that the dependent of current versus distance *d* can be evaluated. As shown in Figure 2d, current flows across the heterrojunction is exponentially decrease with the increase of distance *d*, as consistent to a graph plotted in a logarithmic scale (Figure 2f). This result suggests that current is not a simple linear dependent of distance *d*., i.e., not due to the resistance of the BNNT.

The gate effect on the graphene-BNNT heterojunction was evaluated. As shown in Figure S8h, the potential from the back gate is shielded by the metallic graphene sheet.

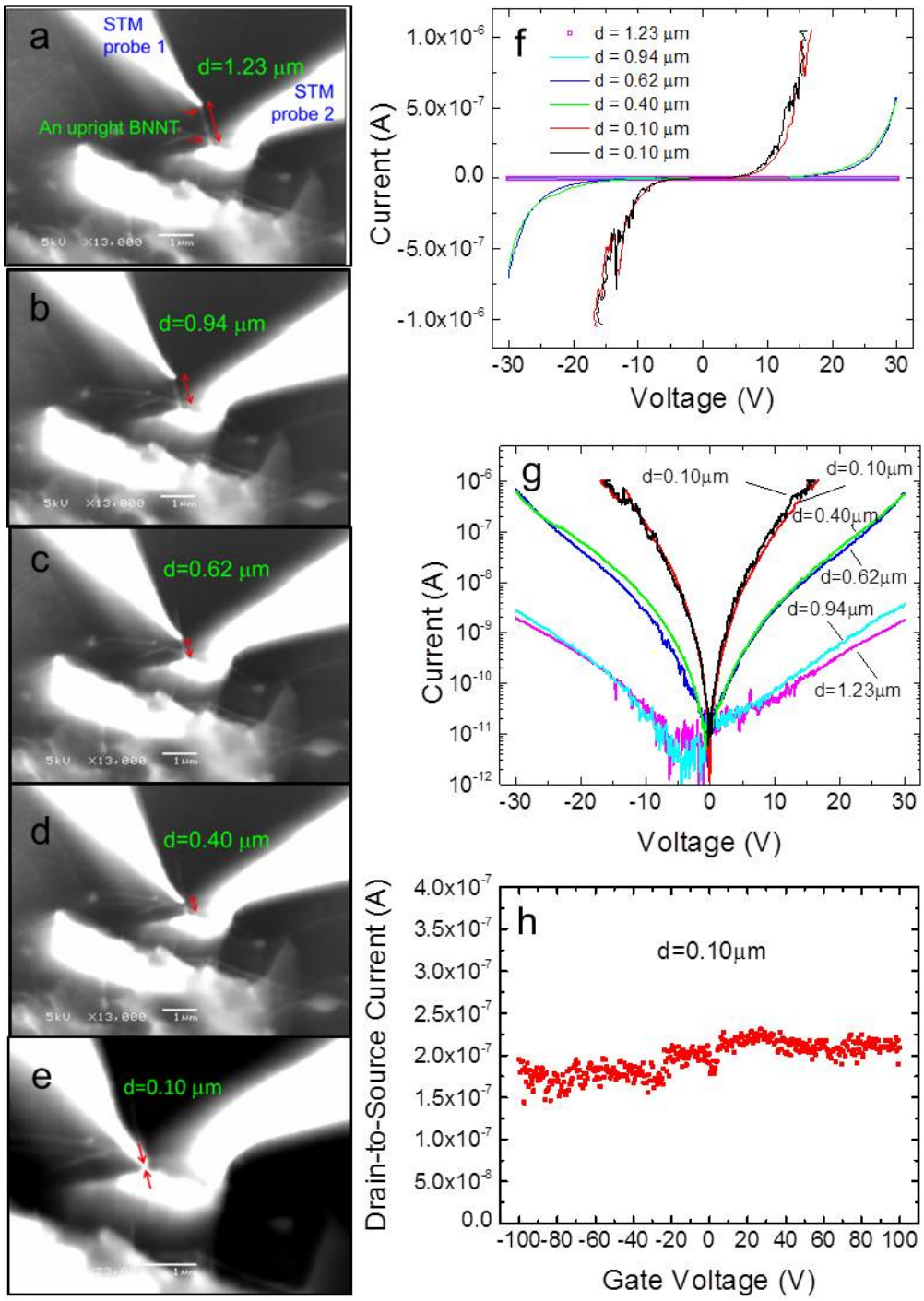

Figure S8: The full data set for *I-V* characteristic across a vertical grephene-BNNT heterojunction.

5. Theory

Electronic structure calculations based on Density Functional Theory (DFT)[4,5] were performed using the SIESTA code. We used the Gradient Generalized Approximation (PBE-GGA) [6] for the exchange-correlation functional. The valence electrons of Kohn-Sham wave-functions were expanded with double-ζ polarized (DZP) basis set. The norm-conserving pseudo-potentials [7] were used for the core electrons. For the geometry optimization, we used a grid of (12x12x1) k-points and the structures were fully relaxed with residual forces in each component of the atoms smaller than 0.01 eV/Å. DOS was calculated using the grid of (100x100x1) k-points. The non-equilibrium Greens Functions (NEGF) method was used to calculate the current-voltage characteristics using the TranSiesta code. [8]

A supercell for graphene was considered with dimensions of 20.24 X 20.24 Å. A BN nanotube with a length of 12 Å was placed perpendicular to the graphene sheet. Firstly, the equilibrium configuration for the pristine graphene and the BN nanotube was obtained. Next, both systems were placed together to form a graphene-BNNT heterojunction. At the BNNT side of the heterojunction, four C atoms were substituted with 2 N and 2 B atoms. The opposite end of the BNNT was passivated with H atoms to avoid the spurious electronic states associated with the dangling bonds. The heterojunction configuration was then optimized, and DOS and electron transport calculations were performed.

The first and second layers of isoplane electron charge distribution at the graphene-BNNT heterojunction are shown in Figure S9. There is a non-negligible charge interaction between graphene and the first layer of BNNT (green color with red/orange localized spots). Electron charges are more localized on the N atoms. For the second isoplane, the uniform red color represents negligible interaction, i.e., there is no mutual influence from the graphene to the

second plane of BN atoms of the BNNT. Apparently, DOS of the graphene have been modified at by the heterojunction but not on the BNNTs.

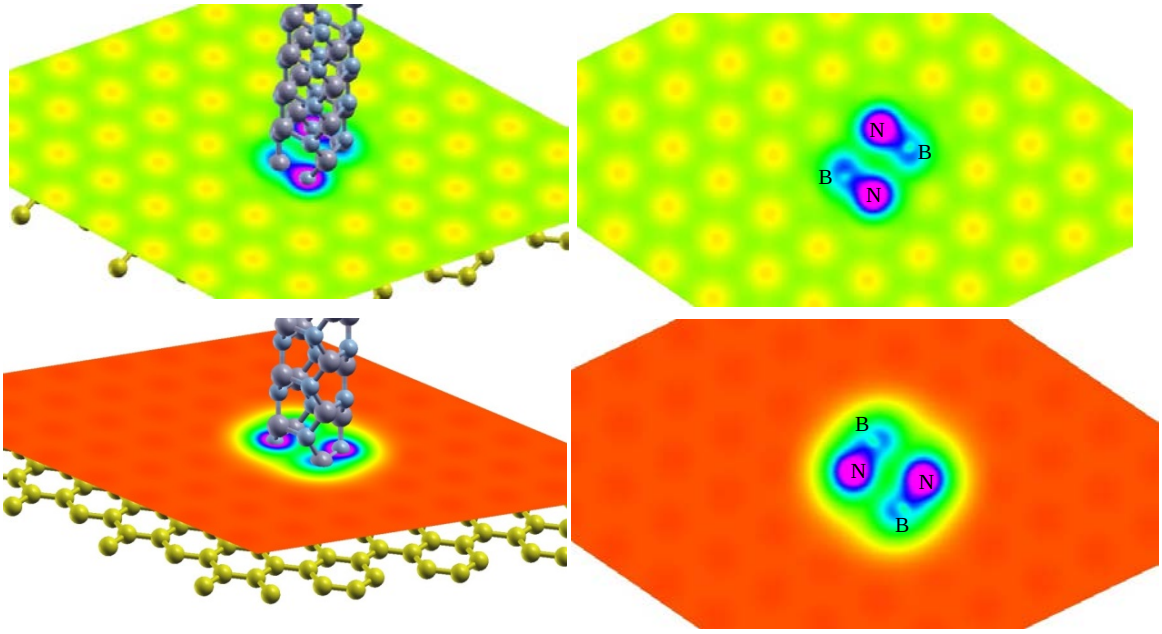

Figure S9. The first (green) and second (red) layer of isoplane electron charge distribution at the graphene-BNNT heterojunctions

References

1 Mohiuddin, T. M. G. *et al.* Uniaxial strain in graphene by Raman spectroscopy: G peak splitting, Gruneisen parameters, and sample orientation. *Physical Review B* **79**, 205433 (2009).

2 Ferrari, A. C. & Basko, D. M. Raman spectroscopy as a versatile tool for studying the properties of graphene. *Nat Nanotechnol* **8**, 235-246 (2013).

3 Calizo, I., Bejenari, I., Rahman, M., Liu, G. & Balandin, A. A. Ultraviolet Raman microscopy of single and multilayer graphene. *J Appl Phys* **106**, 043509 (2009).

4 Hohenberg, P. & Kohn, W. Inhomogeneous Electron Gas. *Physical Review* **136**, B864-B871 (1964).

5 Kohn, W. & Sham, L. J. Self-Consistent Equations Including Exchange and Correlation Effects. *Physical Review* **140**, A1133-A1138 (1965).

6 Perdew, J. P., Burke, K. & Ernzerhof, M. Generalized Gradient Approximation Made Simple. *Physical Review Letters* **77**, 3865-3868 (1996).

7 Troullier, N. & Martins, J. L. Efficient pseudopotentials for plane-wave calculations. *Physical Review B* **43**, 1993-2006 (1991).

8 Brandbyge, M., Mozos, J.-L., Ordejón, P., Taylor, J. & Stokbro, K. Density-functional method for nonequilibrium electron transport. *Physical Review B* **65**, 165401 (2002).